Isotopic Studies of Contaminant Transport at the Hanford Site, WA.

John N. Christensen[1]

Mark E. Conrad[1]

Donald J. DePaolo[1,2]

P. Evan Dresel[3]

[1]Center for Isotope Geochemistry, Earth Sciences Division, E.O Lawrence Berkeley National Laboratory, 1 Cyclotron Rd., Berkeley, CA 94720

[2]Department of Earth and Planetary Science, University of California, Berkeley, CA 94720

[3]Pacific Northwest National Laboratories, Richland, WA 99353

Vadose Zone Journal

Abstract

Processes of fluid flow and chemical transport through the vadose zone can be characterized through the isotopic systematics of natural soils, minerals, pore fluids and groundwater. In this contribution, we first review our research using measured isotopic variations, due both to natural and site related processes, of the elements H, O, N, Sr and U, to study the interconnection between vadose zone and groundwater contamination at the Hanford Site in south-central Washington. We follow this brief review with a presentation of new data pertaining to vadose zone and groundwater contamination in the WMA T-TX-TY vicinity. Uranium (U) isotopic data for the C3832 core (WMA TX) indicates the involvement of processed natural U fuel, and links the observed U contamination to the nearby single shelled tank TX-104. The data also precludes contamination from an early 1970's TX-107 leak. In the case of the C4104 core (WMA T), the U isotopic data indicates a mixture of processed natural and enriched U fuels consistent with the major leak from T-106 in 1973. Uranium and Strontium isotopic data for the cores also provides direct evidence for chemical interaction between high-pH waste fluid and sediment. Isotopic data for groundwater nitrate contamination in the vicinity of WMA-T strongly suggests high-level tank waste (most likely from T-106) as the source of very high ^{99}Tc concentrations recently observed at the NE corner of WMA-T.

Introduction

In 1942 Hanford, Washington was selected as the site for major plutonium production based on its relative isolation and its proximity to the Columbia River, which provided ample power from the Grand Coulee Dam and cooling water for nuclear reactors and Pu separation operations (Smyth 1945). From the time of WWII-era production through the Cold War and eventual end of Pu production in 1987, over 100,000 metric tons of uranium fuel was processed through the reactors and chemical separation processes (DOE/RL-98-48, 1999). High-level radioactive waste resulting from these processes was stored in tank "farms" located in the 200 East and 200 West areas on the Hanford plateau (Figure 1). Leaks and spills associated with many of these tanks together with lower level radioactive waste released directly to the subsurface has left a legacy of vadose zone and groundwater contamination at the site. Some of this contamination has reached the Columbia River, whereas most of it is still resident in the 50 to 100-meter thick vadose zone. There remains the potential for further contaminant migration from the vadose zone to groundwater, and ultimately to the river. Understanding the fate and transport of contaminants has been complicated by the presence of multiple potential sources within

relatively small areas. We have developed and implemented a suite of isotopic techniques, using the elements H, O, N, Sr and U, to study the interconnection between vadose zone and groundwater contamination at the Hanford Site. We demonstrate the use of isotopic measurements to establish sources of contamination and place constraints on the rates of transfer through the vadose zone to groundwater. Our multiple-isotopic system approach has proved to be a powerful means to identify sources of contaminants and, once the sources are identified, to understand the subsurface transport routes and mechanisms.

In this paper we review recent results from isotopic research concerning the Hanford Site conducted at the Center for Isotope Geochemistry (Lawrence Berkeley National Laboratory). New data are presented that relate to vadose zone contamination in the Waste Management Areas (WMA's) T and TX-TY and the source of ^{99}Tc groundwater contamination in the vicinity of the WMA-T.

Geology and Hydrology of the Hanford Site

The Hanford Site is situated on the Columbia Plateau within the Pasco Basin, which was formed by broad folding and faulting of the Miocene-aged Columbia River Basalt Group and overlying sediments. The Pasco Basin is filled with a series of sediments that unconformably overly the Miocene basalts (Hartman et al. 2000). Immediately above the unconformity are Pliocene fluvial and lacustrine deposits of the Ringold Formation, consisting of gravels, silts and clays. At the top of the Ringold Formation is the Cold Creek Unit, a zone of pedogenic carbonate that developed in response to arid climate conditions (Slate 1996). During the Pleistocene the informally designated Hanford formation was deposited by a series of episodic floods resulting from catastrophic failures of ice dams holding back Glacial Lake Missoula located 200 km to the northeast (Bretz 1969, Waitt 1984). The Hanford formation comprises unconsolidated sediments of generally granitic and basaltic provenance ranging in grain size from gravel, through sand to silt. The Hanford formation is overlain by discontinuous Holocene eolian and fluvial deposits. To accommodate the tank farms, the top 10-15 m of the Hanford formation was excavated and backfilled once tank construction was complete.

The basalt ridges (Rattlesnake Hills/Yakima Ridge) along the southwest edge of the Hanford Site are the primary source of natural groundwater recharge for the site along

with diffuse infiltration through the vadose zone (Gee et al. 1992). Groundwater flows through the unconfined aquifer from the basaltic ridges generally eastward through the sediments of the Ringold Formation and Hanford formation, then enters the Columbia River along the eastern side of the site. In addition, there are a stacked series of confined aquifers within the Columbia River Basalt Group, which locally communicate with the overlying unconfined aquifer.

Sedimentary structure has a significant effect on the fluid transport of contaminants in the vadose zone and groundwater (Serne et al. 2004a). Clastic dikes potentially provide cross cutting pathways for contaminant movement. In the sedimentary column within the vadose zone, local highs in moisture content are associated with boundary zones between layers of contrasting grain size. These capillary barriers can generate lateral movement of fluids, especially during times of high fluid flux through the vadose zone. Preferential pathways are also developed through coarser-grained units during high flow. Under low fluid flux conditions, the dominant pathways for fluid transmission are fine-grained layers where water content is highest.

Review of recent isotopic studies

1. Groundwater Sr isotope patterns

The Sr isotopic patterns in groundwater at Hanford site are a good starting point for discussion. Using Sr isotopic analyses of 273 groundwater samples of the unconfined aquifer, Singleton et al. (2006) produced a highly detailed groundwater map of the variation of $^{87}Sr/^{86}Sr$ across the Hanford site (Fig. 1). These data provide a means of tracking groundwater sources, including the water in contaminant plumes, independent of the contaminants themselves. The Sr isotopic composition of groundwater is also sensitive to infiltration through the vadose zone, weathering of the host sediments, and to communication with the deeper confined aquifers within the Columbia River Basalts. This large data set provides an assessment of the evolution of the undisturbed natural groundwater/vadose zone system, as well as the effects of perturbations to groundwater by industrial processes at the site and remediation activities (Singleton et al. 2006).

The groundwater $^{87}Sr/^{86}Sr$ map reflects known aspects of the hydrology and geology of the Hanford Site (Singleton et al. 2006) and provides new insights about the sources of

the present groundwater and broad-scale diffuse infiltration rates. The basalt ridges (Rattlesnake Hills/Yakima Ridge) along the southwest edge of the Hanford Site are the primary sites of groundwater recharge, and due to the relatively low $^{87}Sr/^{86}Sr$ of basalts (0.704 to 0.707), the freshly infiltrated waters initially take on a low $^{87}Sr/^{86}Sr$ ratio. As groundwater moves to the east it exchanges strontium with sediments that have higher $^{87}Sr/^{86}Sr$ (~0.712), while simultaneously obtaining additional diffuse recharge from the vadose zone, which also has relatively high $^{87}Sr/^{86}Sr$. The resulting spatial pattern is gradually increasing $^{87}Sr/^{86}Sr$ from west to east across the site along the lines of groundwater flow (Fig. 1). Superimposed on this general pattern are local effects of both natural and industrial origin. Two areas of low $^{87}Sr/^{86}Sr$ to the north and south of Gable Mt. reflect upwelling of deep groundwater with low $^{87}Sr/^{86}Sr$ from basalt-hosted confined aquifers. Infiltration of Columbia River water ($^{87}Sr/^{86}Sr \approx 0.714$) along the shore of the 100-B,C, -K, -N Areas produces increases in groundwater $^{87}Sr/^{86}Sr$. In contrast, infiltration of Yakima River water ($^{87}Sr/^{86}Sr \approx 0.707$) causes lowering of groundwater $^{87}Sr/^{86}Sr$ to the west of the Richland North area. Surface application of Columbia River water to recharge ponds in the Richland North area produces a strong local high in $^{87}Sr/^{86}Sr$. In the 200 West and 200 East Areas large volumes of process water were discharged to trenches, cribs and ponds, producing major disturbances of water table elevation, and pronounced local highs in groundwater $^{87}Sr/^{86}Sr$ as result of rinsing or stripping of high $^{87}Sr/^{86}Sr$ strontium from the vadose zone (Singleton et al. 2006, Maher et al. 2003).

2. Isotopic Constraints on Vadose Zone Processes

A major factor in the rate of contaminant migration within the vadose zone, and hence the timescale for eventual contamination of groundwater, is the rate of fluid infiltration through the vadose zone. Isotopic data derived from vadose zone fluids and sediments can be used to place constraints on this rate as well as on the rate of weathering of sediments. Maher et al. (2003, 2006) measured and modeled Sr and U isotopic profiles of pore fluids and sediments in an uncontaminated core (now well 299-W22-48) taken in the 200 West Area to the east of WMA-S-SX. The Sr and U isotopic compositions of pore water vary systematically down core. In the case of Sr, decreasing $^{87}Sr/^{86}Sr$ with

depth is a response to progressive weathering of the sediment that releases Sr of lower $^{87}Sr/^{86}Sr$. For U, $^{234}U/^{238}U$ (or activity ratio) generally increases down core, reflecting opposing effects of alpha recoil loss of ^{234}U, which tends to increase pore water $^{234}U/^{238}U$, and chemical weathering that tends to lower the pore fluid isotope ratio toward the secular equilibrium $^{234}U/^{238}U$ activity ratio of unity. For both Sr and U, the isotopic ratios are affected by the infiltration rate through the vadose zone.

Maher et al. (2003) modeled the Sr isotopic data to constrain the ratio of the infiltration rate to the weathering rate, and thus with an assumed range of weathering rates based on studies of other soils estimated an infiltration flux of 7±3 mm/yr. Combining the constraints imposed by both the Sr and U data allows for simultaneous estimation of both the infiltration and weathering rates. Using this analysis, Maher et al. (2006) estimated a long-term (at least 100's of years) infiltration rate of 5±2 mm/yr, and a long-term bulk weathering rate of between $10^{-15.7}$ to $10^{-16.5}$ mol/m^2/sec.

Information from the $^{87}Sr/^{86}Sr$ groundwater map described above can be use to provide model estimates for infiltration fluxes over wider areas. Singleton et al. (2006) used a 1-D model along a line extending ~20 km east-west through an undisturbed portion of the Hanford Site to estimate variation in the infiltration flux. The modeling results suggested, for a constrained value of the dissolution rate in the aquifer of $10^{-7.5}$ yr^{-1}, infiltration fluxes of 0-1.4 mm/yr near the western end at Dry Creek Valley, with infiltration fluxes perhaps as high 30 mm/yr in the central part of the site. These estimates are in general accord with those based on vegetation and soil type (Gee et al. 1992, Fayer and Walters, 1995).

Competition within the soil zone between evapotranspiration and infiltration imposes a profile in pore water $\delta^{18}O$ that can be measured and modeled to elucidate these processes (DePaolo et al. 2004, Singleton et al. 2004). Vadose zone pore fluids deeper than ~2 m in an uncontaminated, relatively undisturbed core (299-W22-48) have essentially constant enrichments in $\delta^{18}O$ of 2 to 4‰ relative to winter precipitation. Pore fluids in the upper 2 meters vary strongly in $\delta^{18}O$ with both depth and season. Modeling suggests that the magnitude of the overall vadose zone $\delta^{18}O$ shift varies inversely with infiltration rate, which in turn is highly dependent on soil type and vegetation. The

results of these studies indicate that diffuse vadose zone drainage increases the $\delta^{18}O$ of groundwater. Thus natural vadose zone fluids (high $\delta^{18}O$) are distinguishable from process water derived from the Columbia River (low $\delta^{18}O$), so that fluids from leaking pipes and surface discharge can be distinguished from natural waters. In the 299-W22-48 core there is evidence of lateral introduction of low-$\delta^{18}O$ process water, elevated levels of tritium (DePaolo et al. 2004) and possibly ^{99}Tc (Serne et al. 2002).

3. Isotopic Signatures of Contamination

One of the great ongoing challenges at the Hanford Site is the identification of the sources of subsurface contamination. Because there are typically many possible contaminant sources within a limited area, such as tank leaks, tank related spills, cribs, trenches, and because each source was active at different times and has different chemical characteristics, it is difficult to determine by what pathway, and at what rates, the contaminants were transported through the vadose zone to groundwater. An even greater challenge is to predict whether, when, and where additional contaminants may start arriving at the water table in the future.

An obvious target for contamination fingerprinting is processed uranium. Uranium from nuclear industrial activities has a wide range of $^{235}U/^{238}U$ and $^{236}U/^{238}U$ due to variable combinations of isotopic enrichment and transformations during the operation of uranium-fueled nuclear reactors. In contrast, natural background uranium has constant $^{235}U/^{238}U$, virtually zero $^{236}U/^{238}U$, but variable $^{234}U/^{238}U$ due to alpha recoil effects. The contrasts in isotopic composition between natural and processed uranium, as well as the wide compositional range of processed uranium, provide the means to trace contaminant uranium in the environment and delineate the sources and history of contamination.

Christensen et al. (2004) used high-precision U isotopic measurements ($^{234}U/^{238}U$, $^{235}U/^{238}U$, $^{236}U/^{238}U$) to investigate the source of groundwater U contamination seen in the early 1990's in the vicinity of the 200 East Area WMA-B-BX-BY. By comparing the U isotopic compositions of groundwater samples to that of porewater samples from two cores (299-E33-41 and 299-E33-46) through vadose zone U contamination, the source of the groundwater contamination was shown to be consistent with an event in 1951 during

which tank BX-102 was overfilled. The association of the groundwater contamination with the BX-102 overfill requires that the U did not migrate just vertically downward 40 meters through the vadose zone, but instead had a component of lateral travel of as much as ~150 m before reaching the water table. The lateral transport is consistent with the large size of the spill and the local geological structure. Furthermore, the observations indicate that groundwater U contamination can appear decades (at least 40 years in this case) after being released to the vadose zone, confirming the downward migration of contaminants in the presence of infiltrating fluids, and the difficulties of predicting transport paths in heterogeneous geologic media subject to extreme hydrological conditions.

Nitrate is a widespread groundwater contaminant at the Hanford Site with groundwater concentrations locally reaching over 1000 ppm, and with 75 km^2 of the unconfined aquifer above the EPA drinking water limit of 45 ppm (Hartman et al. 2006). Possible sources for this contamination include high-level radioactive waste from leaking tanks or cribs, low-level waste derived from site activities, and leaching of naturally occurring nitrate from soils and caliche layers within the vadose zone. Recent development of an isotopic analysis technique involving a bacterially mediated process for preparation of nitrate samples has allowed the rapid analysis of the $\delta^{15}N$ and $\delta^{18}O$ of small amounts of nitrate (Sigman et al. 2001, Casciotti et al. 2002). Singleton et al. (2005) applied an adapted version of this technique to groundwater and vadose zone pore water samples for the analysis of both $\delta^{15}N$ and $\delta^{18}O$ of dissolved nitrate. Nitrate associated with high-level waste is characterized with high $\delta^{15}N$ (>10‰) and normal $\delta^{18}O$ (~5‰). Low-level waste nitrate has high $\delta^{18}O$ (>10‰) with low-to-normal $\delta^{15}N$ (<5‰), while naturally occurring vadose zone nitrate has low $\delta^{18}O$ (<3‰) and low $\delta^{15}N$. These results provide a signature for nitrate source identification where concentrations alone would not be a distinguishing factor. This nitrate isotopic tracing technique is particularly valuable for identifying potential high-level waste plumes as nitrate is a nearly conservative tracer of water movement in the vadose zone and groundwater, and can be used to identify possible problem areas where no radioactive contamination (e.g., U) may yet be evident due to retardation.

New results from WMA-T and WMA-TX-TY

1. Sample collection and background

The WMA-T and WMA-TX-TY tank farms are located within the 200 West Area in the central portion of the Hanford Site. WMA-TX-TY is located due south of WMA-T and consists of the contiguous TX and TY single-shell tank farms. Three boreholes, C3830, C3831 and C3832, (Fig. 2) were drilled in 2003 to evaluate possible leaks from single shell tanks TX-105, TX-107 and TX-104 (Serne et al. 2004a). We analyzed a set of vadose zone samples from C3832 near tank TX-104 for the U and Sr isotopic compositions of porefluids.

Two vadose zone cores were taken in the WMA-T in 2003 (Fig. 2), C4104 just to the SE of the single shell tank T-106, and a second, C4105, just to the SW (Serne et al. 2004b). Tank T-106 was involved in a major event in 1973 in which 435,000 L of high-level waste leaked to the vadose zone over a seven-week period (Routson et al. 1979). Tank T-103 is suspected to have leaked, while T-101 was reported to have been overfilled in the 1960's and to have had a leaky inlet port in 1969 (Jones et al. 2000). We analyzed pore water from vadose zone samples from the C4104 core for U and Sr isotopes. This core has been identified as having the higher U pore water concentrations of the two cores (Serne et al. 2004b).

Groundwater samples analyzed for Sr and nitrate isotopic composition come from monitoring wells in the vicinity of WMA-T (Fig. 2, Table 2). Sampling was conducted in conjunction with the Hanford Groundwater Monitoring Program and occurred in May-June 2005. These samples supplement samples analyzed by Singleton et al. (2005, 2006). Groundwater under WMA-T is contaminated with carbon tetrachloride, chromium, nitrate, ^{99}Tc and tritium, representing local and dispersed contamination from disposal cribs and trenches as well as leaks from single-shell tanks and transfer lines (Hartman et al. 2006). In particular, increasing ^{99}Tc concentration in monitoring well 299-W11-39 (to 27,000 pCi/L in 2005) near the northeast corner of the WMA-T area prompted the emplacement of a new well, 299-W11-25B, (Fig. 2), during which depth discrete samples were collected to 51 m below the groundwater surface. The depth profile from 299-W11-25B revealed high ^{99}Tc concentrations peaking at 182,000 pCi/L at about

10 m below the water table (Hartman et al. 2006). We obtained aliquots for isotopic analysis of nine groundwater samples produced by purge-and-pump sampling during the drilling of W11-25B.

2. Analytical Methods

Two sets of groundwater samples were collected; one set for U and Sr in HDPE bottles acidified with Ultrex Nitric acid, and a second filtered into brown glass bottles and un-acidified for nitrate isotopic ($\delta^{15}N$ and $\delta^{18}O$) analysis. Pore water extracts from the vadose zone core samples were obtained by a 1:1 (by weight) deionized water (DI) rinse with centrifugation and filtration. Separate aliquots of the pore water rinses were then used for the U and Sr isotopic analyses. The depths of the analyzed samples from cores C4104 (near T-106) and C3832 (near TX-104) are presented in Table 1.

For isotopic analysis, the uranium was chemically separated from the allotted sample aliquots using TRU-SPEC (Eichrom Industries Inc.) in small volume Teflon columns scaled down from the procedure of Luo et al. (1997). This separation scheme provides column U yields of ≥95%.

The uranium isotopic compositions ($^{234}U/^{238}U$, $^{235}U/^{238}U$ and $^{236}U/^{238}U$) were measured on a Micromass IsoProbe (MC-ICPMS) at LBNL (Lawrence Berkeley National Laboratory). Uranium isotopes 235 and 238 were measured simultaneously on separate Faraday cups, while 234 and 236 were measured on a Daly ion counting system situated behind a wide-angle retardation potential lens. Static simultaneous measurement routines were used, one for $^{235}U/^{238}U$ and $^{234}U/^{238}U$ and a second for $^{236}U/^{238}U$. Corrections for mass fractionation, Daly-Faraday inter-calibration and for any peak-tail under mass 236 were calculated from bracketed analyses of an in-house secular equilibrium natural uranium standard (20 ppb solution of U ore from the Schwartzwalder Mine, CO provided by W. Sharp, Berkeley Geochronology Center). Isotopic compositions were normalized to the natural $^{238}U/^{235}U$ ratio (= 137.88 by convention (Steiger and Jäger 1977) of the standard solution using an exponential mass fractionation law. Sample solutions were introduced to the MC-ICPMS via a desolvation system (Aridus manufactured by CETAC Inc.) equipped with a low uptake micro-concentric nebulizer. Typical precision for $^{235}U/^{238}U$ is ±0.05% 2σ or better, for $^{234}U/^{238}U$ and $^{236}U/^{238}U$ it is ±0.15% 2σ. $^{236}U/^{238}U$

can be measured down to the 10^{-7} range where precision degrades by about a factor of ten with minimum measurable ratio of ~$2x10^{-8}$.

Sr isotopic analyses of vadose zone pore water and groundwater samples were conducted using thermal ionization mass spectrometry (TIMS). Sr for analysis was separated using Sr specific resin (Eichrom Industries Inc.), loading and eluting the sample with 3N HNO_3; then stripping the separated Sr with clean H_2O. The sample was then dried down with a drop of $HClO_4$ and a drop of concentrated HNO_3 in preparation for loading on an outgassed Re filament with 1% H_3PO_4 and a TaCl emitter solution. Sr isotopic analyses on a VG 54 multicollector mass spectrometer were performed using a multidynamic analysis routine, with normalization to $^{86}Sr/^{88}Sr = 0.1194$. The average $^{87}Sr/^{88}Sr$ measured for NBS 987 over the period of analysis was 0.710281±0.000014 (2σ).

The $\delta^{15}N$ and $\delta^{18}O$ of nitrate in the groundwater samples were determined using a denitrifying bacterial species to generate N_2O from dissolved sample NO_3^- (Singleton et al. (2005) adapted from Sigman et al. (2001) and Casicotti et al. (2002)). Sample nitrite/nitrate is low enough that the nitrite contribution to the generated N_2O is negligible. Isotopic analysis of the NO_2 is then conducted with a continuous flow mass spectrometer (Micromass JA Series IsoPrime), and isotopic values corrected to KNO_3 standards (USGS32, USGS34, USGS35 & IAEA-N3). Analytical precisions are 0.5 per mil for both the $\delta^{15}N$ and $\delta^{18}O$ of nitrate. This technique allows analysis of low sample volume (<4 ml) and low concentration samples down to 0.5 mg/L nitrate (Singleton et al. 2005).

3. Results from Vadose Zone Borehole C3832 (WMA-TX)

The pore water U concentrations in core C3832 (near TX-104) outline a vadose zone contamination plume (Serne et al. 2004a), with U concentrations up to 28.5 ppm, peaking just at the contact between the upper and lower Cold Creek units (Figure 3a). Fourteen pore water samples with sufficient U were analyzed for U isotopic composition. The measured $^{236}U/^{238}U$ of the ten samples within the depth range of 18.96 m to 33.6 m fall within a narrow range of 90.12±0.07 ($x10^{-6}$) to 91.37±0.16 ($x10^{-6}$), despite pore water U concentrations varying by a factor of 10 (Fig. 3b). Likewise, the $^{235}U/^{238}U$ of these

samples also fall in a narrow range of 0.0066701±27 to 0.0066877±18 (errors given are 2σ and apply to the last two digits). The pore water U concentrations, 2.7 to 28.5 ppm, are much higher than background values of 0.015 to 0.15 ppm. The near constant U isotopic composition across the central nine samples of the plume (Figure 3a and Table 1) indicate that these U samples represent essentially the U isotopic composition of the pure contaminant, little affected by mixing with background U. The uniformity of the isotopic ratios also suggests a single relatively well-mixed contamination source. The plume boundaries as defined by $^{236}U/^{238}U$ (or $^{235}U/^{238}U$, not shown) are relatively steep, falling to near background values over at most 5 meters on the up-core margin, while on the down-core margin falling to ~1% contaminant U over an interval of 1.2 m before rising again to ~20% contamination in the next 0.2 m interval. Serne et al. 2004a note that the lowest extent of any sort of contamination was probably not reached in this core.

The U isotopic data for C3832 pore water are presented in plots of $^{236}U/^{238}U$ vs. $^{235}U/^{238}U$ (Fig. 4a) and $^{236}U/^{238}U$ vs. $^{234}U/^{238}U$ (Figure 4b), which are useful for deducing the character of the contaminant sources. In Fig. 4a, natural background U plots on the x-axis (where $^{236}U/^{238}U = 0$) at a value of $^{235}U/^{238}U$ of 0.0072527±21 (Cowan and Adler 1976, Steiger and Jäeger 1977, Cheng et al. 2000). In Figure 4b, natural background U also plots on the x-axis, but within a wide potential range of $^{234}U/^{238}U$. In natural porewater-rock systems, such as in the vadose zone or the saturated zone, the alpha-recoil effect, through the decay of ^{238}U, leads to the unsupported build-up of ^{234}U in interstitial porefluid compared to solids (Kigoshi, 1971). This results in the common observation in groundwaters (Osmond and Cowart 1992, Porcelli and Swarzenski 2003, and references therein) of $^{234}U/^{238}U$ higher than the secular equilibrium value of 54.89 ($x10^{-6}$) (Chen et al. 2000). In contrast, after timescales of 10^6 years, the bulk solid remains close to secular equilibrium, while the outer 10's of nanometers of grains and small (<40 microns) grains tend to become strongly depleted in ^{234}U, and so have $^{234}U/^{238}U$ distinctly less than 54.89 ($x10^{-6}$) (Maher et al. 2006, DePaolo et al. 2006).

In Fig. 4a the data for the ten central samples of the C3832 U plume form a tight cluster on the line representing the array of Hanford processed natural U fuels (Dresel et

al. 2002, Christensen et al. 2004). The remaining four samples (at depths of 13.7m, 18.5 m, 34.9 m and 35.1 m fall along this line toward the composition of natural U, indicating dilution by admixed background U. In Fig. 4b, the ten central samples also form a cluster on the array for processed natural U fuels (Christensen et al. 2004). While the shallowest analyzed sample (13.66 m) has a small excess of ^{234}U ($^{234}U/^{238}U$ activity ratio = 1.051±0.001) the remaining three samples fall very close to the natural U fuels array.

For the C3832 core, nineteen pore water samples were analyzed for Sr isotopic composition. The pore water Sr concentration in the C3832 core ranges from 0.1 to 4 ppm, sharply increasing after a depth of 29 m correlating with an increase in $CaCO_3$ (Serne et al. 2004a). The measured $^{87}Sr/^{86}Sr$ ratios are between 0.7136 and 0.7168, showing no obvious relationship to pore water Sr concentration.

4. Results from Vadose Zone Borehole C4104 (WMA-T)

The pore water U concentrations in the C4104 core are as high as 17.8 ppm, 60% of the highest concentration in the C3832 core (Serne et al. 2004b). The zone of elevated U concentration extends from 14.32 m to 28.23 m depth where the range of 1.15 ppm to 17.8 ppm U is 15 to >200 times greater than the background porewater U concentrations (Figure 3b). Measured $^{236}U/^{238}U$ ratios in samples within the elevated U concentration plume are between 100.65±0.11 ($x10^{-6}$) and 184.08±0.30 ($x10^{-6}$), reaching values twice as high as in the C3832 core (Figure 3b). The overall trend down-core, with one reversal at 92.6 feet, is of decreasing $^{236}U/^{238}U$. This is in contrast to the relatively uniform isotopic composition across the U plume in the C3832 core. The two deepest analyzed pore water samples in C4104, at 30.89 m and 32.74 m, have low U concentrations but still measurable $^{236}U/^{238}U$ (0.115 ppm, 38.027±0.093 ($x10^{-6}$) and 0.053 ppm, 0.941±0.012 ($x10^{-6}$) respectively).

The U isotopic data for C4104 are also plotted in Figure 4a ($^{236}U/^{238}U$ vs. $^{235}U/^{238}U$) and Figure 4b ($^{236}U/^{238}U$ vs. $^{234}U/^{238}U$). In Figure 4b, all the samples plot off the line representing processed natural U fuels. The four shallowest analyzed samples form a short array between Hanford processed enriched fuels and the array of natural U fuels. The positions of these data points along a best-fit line imply that the contaminant in C4140 consisted of no more than 16% processed enriched U fuel. The spread of the

data for these four samples suggests that the proportion of processed enriched U decreases by 2 to 3% down core over the depth interval 14.3 to 23.2 m. The composition of the processed natural U end-member is indicated by the intersection of the best-fit line with the array of natural U fuels and has a $^{236}U/^{238}U$ of approximately $120x10^{-6}$, and a $^{234}U/^{238}U$ of $\sim 53x10^{-6}$ (Figure 4b). In Figure 4a ($^{236}U/^{238}U$ vs. $^{235}U/^{238}U$) the remaining five samples (depth interval 24.7 to 32.7 m) must fall along a fanning set of mixing lines projecting from the singular composition of natural background U and ending at various points along the line through the samples from the 14.3-23.2 m interval. The segment thus subtended by the fan of mixing lines indicates a greater range in the isotopic composition of the U contaminant than is observed in the four samples from the 14.3-23.2 m depth interval, extending it down to a minimum of 9% processed enriched U fuel.

On Figure 4b, the distribution of the five samples from the 24.7 to 32.7 m interval constrains the range of $^{234}U/^{238}U$ of the natural background U that diluted/mixed with the contaminant U, and so is suggestive of the source (e.g. pore fluid vs. sediment) of the natural U. Using sample C4104-9a (23.2 m depth) as representing the contaminant endmember, a line including it and samples C4104-10a (24.7 m depth) and -11a (26.6 m depth) intersects (at $^{236}U/^{238}U = 0$) the $^{234}U/^{238}U$ axis at 54.74 ± 0.19 ($x10^{-6}$) (±95% confid.), indicating that the natural U end member had a secular equilibrium value for $^{234}U/^{238}U$. For samples C4104-9a, -12a (28.2 m) and -18a (32.7 m), the best fine line indicates a different natural U $^{234}U/^{238}U$ of 56.76 ± 0.09 ($x10^{-6}$), somewhat above the secular equilibrium value. The extreme example in the core is sample C4104-16a (30.9 m depth), its position in Figure 4b requires that the natural U end member $^{234}U/^{238}U$ was significantly below the secular equilibrium value, as low as 50.86 ± 0.07 ($x10^{-6}$) (±95% confid.) if sample -9a is used as the contaminant end member. Even using the minimum of 9% processed enriched fuel suggested above for the contaminant in C4104 (Figure 4a) does not affect the requirement for sample 16a for a component of natural U significantly below secular equilibrium. However, for samples 10a and 11a, it would allow values above but close to secular equilibrium. Still, these values are below the range for vadose pore water observed in the B-BX WMA (Christensen et al. 2004) and a background clean core (Maher et al. 2006) (ranges shown in Figure 4b).

Eighteen pore water samples from core C4104 were analyzed for $^{87}Sr/^{86}Sr$ ratio. Pore water concentrations of Sr ranged from <0.1 ppm to 20 ppm, with the peak in Sr concentration coinciding with peaks in nitrate and ^{99}Tc concentrations (Fig. 5); (Serne et al. 2004b). The $^{87}Sr/^{86}Sr$ of pore water ranges from 0.7112 to 0.7148, and except for the shallowest sample, all are lower than measured in core C3832 pore water samples.

5. Groundwater Data for the WMA-T

Sr isotopic and concentration data for groundwater monitoring wells in the vicinity of WMA-T and WMA-TX-TY are presented in Table 2 and in Figure 6 along with previously published data from Singleton et al. (2006). The resulting map of groundwater $^{87}Sr/^{86}Sr$ highlights two areas near WMA-T of enhanced recharge from the vadose zone indicated by $^{87}Sr/^{86}Sr > 0.710$ (Fig. 6a). One area appears associated with the T-36, T-7 and T-32 cribs, where ~$1.4x10^5$ kL of low-level waste, including nitrate, was disposed to the vadose zone. Monitoring wells reveal very high groundwater nitrate concentrations, up to 3000 ppm near these cribs as well as high Sr concentrations up to 2400 ppb (~10x normal Sr groundwater concentrations). A second area of very high $^{87}Sr/^{86}Sr$ is located just north of WMA-T near the beginning of the 216-T-4-2 ditch which drains dilute process water. Groundwater in this area contains moderately high nitrate (250 ppm) and ^{99}Tc concentrations (140 pCi/L). Near the NE corner of WMA-T, there is moderately high groundwater $^{87}Sr/^{86}Sr$ (>0.7095 and <0.7100). These wells are also associated with very high ^{99}Tc concentrations. The set of discrete depth samples from 299-W11-25B (location shown in Fig. 2) provides a vertical section of the unconfined aquifer in the region of highest ^{99}Tc concentration (Fig. 6b). The samples describe a zone of vertical mixing within the aquifer between Sr with high $^{87}Sr/^{86}Sr$ flushed from the vadose zone and Sr with lower $^{87}Sr/^{86}Sr$ representative of the broader $^{87}Sr/^{86}Sr$ trend for groundwater in the area. This parallels the contrast seen in pairs of adjacent wells drilled to different depths, where groundwater from the deep well has lower $^{87}Sr/^{86}Sr$ than groundwater from the shallow well (Fig. 6a).

Nitrate isotopic data ($\delta^{15}N$ and $\delta^{18}O$, Table 2) for shallow groundwater wells surrounding WMA-T and groundwater samples from the well 299-W11-25B depth

profile are presented in Fig. 7. Most of the WMA-T groundwater samples form an array separate from the array described by the nine discrete depth samples from 299-W11-25B. The two exceptions are samples from wells 299-W11-39 and 299-W10-8, located near the northeast corner of WMA-T and 299-W11-25B. The WMA-T array traverses the region in Fig. 7 between the field representing the composition of synthetic nitrate and the field representing the isotopic composition of naturally occurring nitrate in the vadose zone. The high $\delta^{18}O$ end of the WMA-T array is represented by samples with very high (>900 ppm) nitrate concentrations, including well 299-W10-4 (2420 ppm nitrate), adjacent to the T-36 crib. The low $\delta^{18}O$ end of the array has the lowest nitrate concentrations. These observations suggests that this array represents mixing between synthetic nitrate from low level waste and natural nitrate flushed from the vadose zone. The data for discrete depths in well 299-W11-25B describes a separate trend (Fig. 7) from synthetic nitrate (low-level waste) toward fields representing the isotopic compositions of nitrate from vadose zone samples contaminated by high-level tank related waste. The deepest sample in 299-W11-25B falls at the upper end of the array, closest to the field for low-level waste. This sample also has the lowest ^{99}Tc concentration. The shallowest two samples, including the sample with the highest ^{99}Tc concentration (151,000 pCi/L) fall at the low $\delta^{18}O$, high $\delta^{15}N$ end of the array toward the composition of nitrate from high-level waste. This indicates that nitrate in 299-W11-25A represents variable mixing between high-level and low level sources, and implies that the source of the very high levels of ^{99}Tc seen in the upper part of 299-W11-25B and in the NE corner of WMA-T is from tank-related high-level waste.

Uranium concentrations in the analyzed WMA-T and 299-W11-25B samples are low, less than 2 ppb. Their U isotopic compositions are presented in Table 3. The measured $^{235}U/^{238}U$ ratios of the samples are indistinguishable or very close to the natural ratio. The $^{236}U/^{238}U$ of these samples are all very low, less than $5x10^{-7}$. Both these factors indicate a very low level of contamination by processed U. The contaminant contribution, <1%, is too minor to identify accurately the source of the U contamination. The $^{234}U/^{238}U$ of these six samples are all relatively high ($74.1 x10^{-6}$ to $96.5x10^{-6}$) compared to groundwater in the vicinity of the WMA-B-BX-BY in the 200 East Area (Christensen et al. 2004) and at the location of the 299-W22-48 borehole in the southern

portion of the 200 West Area (Maher et al. 2006) but similar to the value, 98.4×10^{-6}, for a clean well (299-W11-6) situated ~650 m to the SE (Fig. 6).

Discussion

1. Sources and Histories of Contamination for Boreholes C3832 and C4104 Cores

In the C3832 core, collected from WMA-TX-TY, the isotopic composition of the contaminant is consistent with processed *natural* U fuel with a $^{236}U/^{238}U$ as high as 91×10^{-6}. No evidence for a component of processed *enriched* U is seen. These observations place constraints that can be used to infer the source of the contaminant U based on the history of fuel type and usage at the Hanford Site. From a perusal of a model history of processed natural U (Watrous 2002), the first time that T-plant processed fuel reached a $^{236}U/^{238}U$ of $\sim 91 \times 10^{-6}$, was in 1951. Enriched U fuel was not processed until 1958, thus suggesting that either the contamination in C3832 came from a pre-1958 source, or from a source/waste stream that never received processed enriched U. Though it is not listed in site documents as having leaked, single shell tank TX-104, located just south of C3832 (Fig. 2) matches well the above constraints. A possible alternative is the set of trenches arrayed 125 m to the west of WMA-TX. These retention trenches received over 6000 kL of first cycle supernatant via tanks TX-109, TX-110 and TX-111 in order to provide needed tank volume for processed fuel separations (Maxfield 1979). However, the first decontamination cycle waste had considerably lower uranium concentrations than the "metal waste" that contained nearly all the uranium from the extraction (Anderson 1990). Thus the T-21 to T-25 retention trenches are not a likely source of the contamination observed in C3832. Estimate of the isotopic composition of U associated with TX-107 leaks during the period 1975 to 1977 (Jones et al. 2000) are not compatible (Fig. 4) with the apparent lack of processed enriched U in C3832. Myers (2005) presents a scenario where the metal waste loss from tank TX-104 took place during a process to sluice sludge from the tank for recovery of the uranium. Thus the chemistry and mobility of the waste may have been modified during the sluicing process. The uranium isotopic data is consistent with this hypothesis.

The U contamination in C4104 in the WMA-T, as described above, represents a mixture of processed natural U and processed enriched U, in roughly the proportions of

85% and 15% respectively. In detail the proportion of processed enriched U appears to decrease down hole from 16% to 9%, suggesting that contamination came from a source that was not perfectly well mixed, or that the composition of the source changed somewhat with time during the leak event. The inferred compositions of the two contaminant end members places some constraints on the time frame of the contamination. From the line through the shallowest four samples, the processed natural U component had a $^{236}U/^{238}U$ of ~$120x10^{-6}$, while the processed enriched U component had a $^{236}U/^{238}U$ of approximately $525x10^{-6}$. These values are both consistent with processed enriched U in the late 1960's (Watrous, 2002). No natural U fuel was processed in 1970, while the batches run in 1971-1972, the last years of the use of natural U fuel, never reached a $^{236}U/^{238}U$ level greater than $95x10^{-6}$. The material leaked in 1973 from T-106 originated from fuel rods processed as much as five years before the event (Rouston et al. 1979 see appendix G) and so is compatible with the broad time frame indicated by the U isotopic observations in C4104. Mixing within the vadose zone of the T106 leak fluids with fluids from a nearly contemporaneous leak at T-103 is a possible explanation of the range seen in C4104, but though the estimated U concentrations are similar for the two leaks (Jones et al. 2000), the leak volume for T-106 and hence the mass of U involved was 40 times greater. An alternate explanation is that the leak changed composition with time. The 1973 T-106 incident occurred during the transfer of supernatant to T-106 via cascade flow by pumping the supernatant first into tank T-105 (Rouston et al. 1979), probably causing some time dependent mixing amongst the contents of T-105, T-106 and the newly added supernatant. This would have produced a non-constant U isotopic composition to the contaminant fluid that percolated downwards at the location of C4104, producing the isotopic range observed down core over the 14.3-23.2 m depth interval.

2. Isotopic Evidence for Sediment-Contaminant Fluid Interaction

The U and Sr isotopic compositions of vadose zone pore water in cores C4104 and C3832 presented above provide evidence of chemical interaction of contaminant fluids with sediment. In Figure 8, for C4104 $^{236}U/^{238}U$ shows a correlation with pH, indicating that as the extreme pH of the contaminant fluid was reduced or neutralized, the

contaminant U was diluted by natural composition U with $^{236}U/^{238}U = 0$. Wan et al. (2004a,b) show that high pH (~14) tank supernatant will react with Hanford sediment silicates in a chemical process that reduces pH in the main plume, while pushing ahead a front of high Ca, Mg, etc. pore fluid concentrations resulting from cation exchange due to high Na^+ contaminant fluid (Serne et al. 2004b). This front would likely be accompanied by mobile contaminants such as nitrate and ^{99}Tc. As described above, C4104 samples (10a, 11a, and 16a) in the lower portion of the core, likely represent mixing between the U contaminant and background natural U with $^{234}U/^{238}U$ ratio just near, to well below in the case of 16a, the secular equilibrium value. With time the alpha-recoil effect imparts distinctive $^{234}U/^{238}U$ signatures to sedimentary material and pore water/groundwater that can be used to distinguish between simple mixing between contaminant fluids and pore fluids, versus chemical interaction between the contaminant fluid and the host sediment. For C4104 samples 10a and 11a, the near secular equilibrium $^{234}U/^{238}U$ ratio of the natural U end member is consistent with wholesale release of U from the bulk sediment as a result of the reaction between the high pH fluid and sediment. Sample 16a presents an extreme value of $^{234}U/^{238}U$ for the natural U component, significantly below the secular equilibrium value. This is consistent with release of U from the outer edges of grains or from fine-grained material (Maher et al. 2006). Interestingly, sample 16a consists of a sandy mud (Serne et al. 2004b), providing a fine-grained source material for low $^{234}U/^{238}U$.

Though no high pH was observed in C3832 (Serne et al. 2004a), samples 121B, and 61B fall on or just to the left of the natural U fuel line in Fig. 4b suggesting some interaction between contaminant fluid and sediment. This suggests the initial occurrence of high pH in the contaminant plume seen in C3832, and would thus emphasize the unreliability of pH as an indicator of the involvement of tank waste since pH can be altered (Wan et al. 2004a,b; Serne et al. 2004b).

Further evidence for contaminant/sediment interaction is provided by the Sr isotopic profiles of C4104 and C3832. In Figure 9 they are compared to the $^{87}Sr/^{86}Sr$ profile of the 299-W22-48 core (Maher et al. 2003), which showed minimal impact from site contamination. Both the C4104 and C3832 profiles appear shifted in $^{87}Sr/^{86}Sr$ toward

the range of bulk sediment and away from the clean core profile, with the shift for C4104 being the greatest. This suggests the release of relatively low $^{87}Sr/^{86}Sr$ from the whole rock or feldspars (Figure 9) due to interaction with the contaminant fluid. In detail, the greatest apparent $^{87}Sr/^{86}Sr$ shift in C4104 occurs within the zone of elevated pH (> ~9 between 14 and 28 m depth). At the peak of pore water ^{99}Tc and Sr concentrations (Sr = 20 ppm at 35.4 m depth, Fig. 5), there is a local high in $^{87}Sr/^{86}Sr$ (=0.7123) perhaps reflecting Sr released from clays in the ion exchange process that produced the high Ca concentration front.

3. Isotopic constraints on the Source of ^{99}Tc Contamination in the Vicinity of WMA-T

The isotopic data for nitrate in groundwater samples from 299-W11-25B indicates that it is derived from a mixture of high-level tank waste and low-level process waste discharged to disposal cribs and trenches. The most likely source of the low-level waste is a plume of groundwater nitrate extending from the southwest corner of the WMA-T area. Simpson et al. (2001) have estimated that $3.6x10^6$ kg of nitrate was discharged to the T-7 and T-32 cribs located in that area (Figure 2). Groundwater samples from the closest monitoring wells to those cribs, 299-W10-4 and 299-W10-28, consistently have the highest nitrate concentrations in the WMA-T area. In addition, the $\delta^{18}O$ values of the nitrate in all these samples are high (up to 15.4‰), indicating a high proportion of synthetic nitrate.

Given the relatively low ^{99}Tc concentrations in these samples (<1000 pCi/L), it follows that most of the ^{99}Tc in 299-W11-25B must be derived from the source of the high-level waste nitrate. The T-106 spill observed in the C4104 core is a likely candidate for the source of the high-level waste contamination. There were several other documented leaks from the T tanks, but this was the largest leak. The T-101 tank (which is closer to the northeast corner of WMA-T) also leaked, but that leak was much smaller volume (<10%) and the concentration of ^{99}Tc in the leak fluids was much lower (~7%).

The net contributions of fluid from the T-106 leak necessary to account for the ^{99}Tc concentrations observed in 299-W11-25B is relatively low. The highest ^{99}Tc concentrations in the C4104 core (between 35 and 39 m depth on Figure 5) range from $4x10^6$ to $25x10^6$ pCi/L, averaging $8x10^6$ pCi/L. At that level, only a 2% contribution to

groundwater from the pore fluids from C4104 would be necessary to produce the highest ^{99}Tc concentration measured in 299-W11-25B. The nitrate concentrations in the peak interval in C4104 range from about 4,500 to 10,500 mg/L averaging about 6,000 mg/L. 2% of the average composition would be 120 mg/L, or only about 21% of the nitrate concentration observed in the C4104 sample with the peak ^{99}Tc concentration. That implies that the remaining 79% of the nitrate in the peak sample is derived from the low-level groundwater nitrate plume. The amount of T-106 fluids necessary to account for the other samples from 299-W11-25B will all be less (<0.3% for the deepest sample).

The suggestion that the T-106 spill as the source of contamination may be verified if a sufficient fraction of contaminant U appears in groundwater samples associated with high ^{99}Tc. Chemical retardation of U relative to ^{99}Tc may be delaying the arrival of T-106 contaminant U. However, a 1999 sample from well 299-W10-24 analyzed by Dresel et al. (2002) had a $^{236}U/^{238}U$ of ~$32x10^{-6}$, about ten times the level of the 2005 sample (Table 2). The W10-24 groundwater sample from 1999, plotted in Fig. 4a, is consistent with natural U with ~20% contamination by T-106 U. By the time of the 2005 sample, it appears that this T-106 U had been essentially diluted/flushed away.

Summary and Conclusions

Isotopic studies add an extra dimension to the characterization of subsurface contamination leading to insights into contaminant source and behavior as well as the processes that affect contaminant transport and mobility. Natural strontium isotopic composition ($^{87}Sr/^{86}Sr$) is particularly sensitive to water-rock interaction and show areas of enhanced recharge through elevated $^{87}Sr/^{86}Sr$ in groundwater. The nitrogen and oxygen isotopic compositions of nitrate show distinct contrasts between the attributed high- and low-level waste sources investigated so far. Uranium isotopic measurements can also be useful for understanding water-rock interactions. In addition for the Hanford site, because the U isotopic ratios of potential sources changed through time as a result of varying fuel enrichment and reactor exposure, U isotopic measurements can also be used to identify the source and timing of contamination. Combining multiple isotopic measurements with conventional chemical data, constrains the possible contaminant sources and the transport path and rate in the vadose zone and groundwater.

Our recent studies in WMA T-TX-TY strongly implicate tank-sourced waste, likely the T-106 leak in 1973, in the shallow ^{99}T and nitrate contamination near the northeast corner of WMA-T. The uranium and strontium isotopic data for the C3832 and C4104 cores, and chemical data from previous studies, show varying amounts of interaction between the infiltrating waste fluids and vadose zone sediments. The high pH, high ionic strength tank fluids greatly enhance the reaction with sediments over that of background infiltrating recharge. Even the relatively low levels of uranium contamination seen in the WMA-T and WMA-TX-TY vadose zone cores are sufficient to provide considerable constraints on the source and timing of contamination.

Acknowledgements:

Funding for this study was provided by the Department of Energy under Contract DE-AC02-05CH11231 to LBNL through the Hanford Science and Technology Program, and by the Assistant Secretary of the Office of Environmental Management, Office of Science and Technology, under the Environmental Management Science Program (now Environmental Remediation Sciences Program) of the Department of Energy under Contract DE-AC02-05CH11231 (LBNL) and Contract DE-AC06=76RL01830 (PNNL). The authors gratefully thank the Hanford Groundwater Monitoring Program for providing groundwater samples, as well as Jeff Serne and Clark Lindenmeier for providing core samples.

References

Amberger, A., Schmidtt, H.-L. 1987. Natürliche Isotopengehalte von Nitrat als Indikatoren für dessen Herkunft. Geochim. Cosmochim. Acta. 51:2699-2705.

Anderson, J.D. 1990. A History of the 200 Area Tank Farms. WHC-MR-0132. Westinghouse Hanford Company, Richland WA.

Bretz, J.H. 1969. The Lake Missoula floods and Channeled Scabland. J. Geol. 77:505-543.

Casciotti, K.L., Sigman, D.M., Hastings, M., Bohlke, J.K., Hilkert, A.M. 2002. Measurement of the oxygen isotopic composition of nitrate in seawater and freshwater. Anal. Chem. 74:4905-4912.

Cheng, H., Edwards, R.L., Hoff, J., Gallup, C.D., Richards, D.A., Asmerom, Y. 2000. The half-lives of uranium-234 and thorium-230. Chem. Geol. 169:17-33.

Christensen, J.N., Dresel, P.E., Conrad, M.E., Maher, K., and DePaolo, D.J. 2004. Identifying the sources of subsurface contamination at the Hanford site in Washington using high-precision uranium isotopic measurements. Environ. Sci. Technol. 38:3330-3337.

Cowan, G.A. and Adler, H.H. 1976. The variability of the natural abundance of ^{235}U. Geochim. Cosmochim Acta. 40:1487-1490.

DePaolo, D.J., Conrad, M.E., Maher, K., and Gee, G.W. 2004. Evaporation effects on oxygen and hydrogen isotopes in deep vadose zone pore fluids at Hanford, Washington. Vadose Zone J. 3:220–232.

DePaolo, D.J., Maher, K., Christensen, J.N., McManus, J. 2006. Sediment transport time measured with U-series isotopes: results from ODP North Atlantic Drift Site 984. Earth Planet. Sci. Lett. 248:379–395.

Dresel, P.E., Evans, J.C., Farmer, O.T.,III. 2002. Investigation of isotopic signatures for sources of groundwater contamination at the Hanford site. PNNL-13763. Pacific Northwest National Laboratory, Richland, WA.

Fayer, M.J. and Walters, T.B. (1995) Estimated recharge rates at the Hanford Site. PNNL-10285. Pacific Northwest National Laboratory, Richland, WA.

Gee, G.W., fayer, M.J., Rockhold, M.L. and Campbell, M.D. 1992. Variations in recharge at the Hanford Site. Northwest Science. 66:237-250.

Hartman, M.J., ed. 2000. Hanford Site groundwater Monitoring Setting, Sources and Methods. PNNL-13080. Pacific Northwest National Laboratory, Richland, WA.

Hartman, M.J., Morasch, L.F., Webber, W.D., eds. 2006. Hanford Site Goundwater Monitoring Report for Fiscal Year 2005. PNNL-15670. Pacific Northwest National Laboratory, Richland, WA.

Jones, T.E., Simpson, B.C., Wood, M.I., Corbin, R.A. 2000, Preliminary Inventory Estimates for Single-Shell Tank Leaks in T, TX, and TY Tank Farms. RPP-7218. CH2M HILL Hanford Group, Inc. Richland, WA. 2000

Kendall, C. Tracing nitrogen sources and cycling in catchments. In *Isotope Tracers in Catchment Hydrology*, Kendall, C., McDonnell, J.J., Eds.; Elsevier Science: Amsterdam, 1998, pp519-576.

Kigoshi, K. 1971. Alpha-recoil thorium-234—dissolution into water and uranium-234/uranium-238 disequilibrium in nature. Science. 173:47–49.

Luo, X.Z., Rehkämper, M., Lee, D.C., Halliday, A.N. 1997. High precision Th-230/Th-232 and U-234/U-238 measurements using energy-filtered ICP magnetic sector multiple collector mass spectrometry. Int. J. Mass Spectrom. 171:105-117.

Maher, K., DePaolo, D.J., Conrad, M.E., and Serne, R.J. 2003. Vadose zone infiltration rate at Hanford, Washington, inferred from Sr isotope measurements. Water Resour. Res. 39:1029-1043.

Maher, K., DePaolo, D.J. and Christensen, J.N. 2006. U-Sr isotopic speedometer: Fluid flow and chemical weathering rates in aquifers. Geochim. Cosomochim Acta. 70:4417-4435.

Maxfield, H.L. 1979. Handbook of the 200 Areas Waste Sites. RHO-CD-673, Rockwell Hanford Operations, Richland, WA.

Myers, D.A. 2005. Field Investigation Report for Waste Management Areas T and TX-TY. RPP-23752 Rev. 0a. CH2M HILL Hanford Group, Inc., Richland, WA.

Osmond, J.K. and Cowart, J.B. 1992. Ground water. *In*: Uranium-series disequilibrium. Ivanovich M., Harmon, R.S. (eds) Clarendon Press Oxford, p.290-334.

Porcelli, D., Swarzenski, P.W. 2003. The behavior of U- and Th-seriesnuclides in groundwater. *In*: Uranium-Series Geochemistry, Reviews in Mineralogy and Geochemistry, vol. 52, Mineralogical Society of America, Washington, DC, pp. 317–361.

Routson R.C., Price, W.H., Brown, D.J. and Fecht, K.R. High-Level Waste Leakage from the 241-T-106 Tank at Hanford. RHO-ST-14 Rockwell Hanford Operations, Energy Systems Group, Richland, WA., 1979

Serne, R.J., Schaef, H.T., Bjornstad, B.N., Williams, B.A., Lanigan, D.C., Horton, D.G., Clayton, R.E., LeGore, V.L., O'Hara, M.J., Brown, C.F., Parker, K.E., Kutnyakov, I.V., Serne, J.N., Mitroshkov, A.V., Last, G.V., Smith, S.C., Lindenmeier, C.W., Zachara, J.M., and Burke, D.B. 2002. Characterization of uncontaminated vadose zone sediment from the Hanford Reservation—RCRA borehole core samples and composite samples. PNNL-13757-1. Pacific Northwest National Laboratory, Richland, WA.

Serne, R.J., Lindberg, M.J., Baum, S.R., Bjornstad, B.N., R.E., Clayton, R.E., Geiszler, K.N., Horton, D.G., LeGore, V.L., Valenta, M.M., Lanigan, D.C., Orr, R.D., Vickerman, T.S., Lindenmeier, C.W., Kutnyakov, I.V. 2004a. Characterization of Vadose Zone Sediments Below the TX Tank Farm: Boreholes C3830, C3831, C3832 and RCRA Borehole 299-W10-27. PNNL-14594. Pacific Northwest National Laboratory, Richland, W.A.

Serne, R.J., Lindberg, M.J., Valenta, M.M., Bjornstad, B.N., Clayton, R.E., Kutnyakov, I.V., Horton, D.G., LeGore, V.L., Vickerman, T.S., Lanigan, D.C., Geiszler, K.N., Orr, R.D., Schaef, H.T., Baum, S.R., Brown, C.F., Lindenmeier, C.W. 2004b. Characterization of Vadose Zone Sediments Below the T Tank Farm: Boreholes C4104,

C4105, 299-W10-196, and RCRA Borehole 299-W11-39. PNNL-14849. Pacific Northwest National Laboratory, Richland, W.A.

Sigman, D.M., Casciotti, K.L., Andreani, M., Barford, C., Galanter, M., Bohlke, J.K. 2001. A bacterial method for the nitrogen isotopic analysis of nitrate in seawater and freshwater. Anal. Chem. 73: 4145-4153.

Simpson, B.C., Corbin, R.A. and Agnew, S.F. 2001. Groundwater/vadose zone integration project: Hanford soil inventory model. BHI-01496. Bechtel Hanford, Inc., Richland, WA.

Singleton, M.J., Sonnenthal, E.L., Conrad, M.E., DePaolo, D.J., Gee, G.W. 2004. Multiphase reactive transport modeling of seasonal infiltration events and stable isotope fractionation in unsaturated zone pore water and vapor at the Hanford site. Vadose Zone J. 3:775-785.

Singleton, M.J., Woods, K.N., Conrad, M.E., DePaolo, D.J., Dresel, P.E. 2005. Tracking sources of unsaturated zone and groundwater nitrate contamination using nitrogen and oxygen stable isotopes at the Hanford Site, Washington. Environ. Sci. Technol. 39:3563-3570.

Singleton, M.J., Maher, K., DePaolo, D.J., Conrad, M.E. and Dresel, P.E. 2006. Dissolution rates and vadose zone drainage from strontium isotope measurements of groundwater in the Pasco Basin, WA unconfined aquifer. J. Hydrol. 321:39-58.

Slate, J.L. 1996. Buried carbonate paleosols developed in Pliocene-Pleistocene deposits of the Pasco Basin, south central Washington, USA. Quatern. Interntl. 34-36:191-196.

Smyth, H.D. 1945. Atomic Energy for Military Purposes: The Official Report on the Development of the Atomic Bomb under the Auspices of the United States Government, 1940-1945. Princeton University Press, 264 p.

Steiger, R.H., Jäger, E. 1977. Subcommission on geochronology: Convention on the use of decay constants in geo- and cosmochronology. Earth Planet. Sci. Lttrs. 36:359-362.

Waitt, R.B., Jr. 1984. Periodic jökulhlaups from the Pleistocene glacial Lake Missoula – New evidence from varved sediment in northern Idaho and Washington. Quaternary Research. 22:46-58.

Wan, J., Larsen, J.T., Tokunaga, T.K., and Zheng, Z. 2004a. pH neutralization and zonation in alkaline-saline tank waste plumes. Environ. Sci. Technol. 38:1321-1329.

Wan, J., Tokunaga, T.K. Larsen, J.T. and Serne, R.J. 2004b. Geochemical evolution of highly alkaline and saline tank waste plumes during seepage through vadose zone sediments. Geochem. Cosmochem. Acta. 68:491-502.

Watrous, R.A. 2002. Activity of Fuel Batches Processed Through Hanford Separations Plants, 1944 Through 1989. RPP-13489, Rev. 0. CH2M HILL Hanford Group, Inc., Richland, WA.

Watrous, R.A. and Wootan, D.W. 1997. Activity of fuel batches processed through Hanford separation plants, 1944 through 1989. HNF-SD-WM-TI-794, Lockheed Martin Hanford Corporation, Richland, WA.

Figure Captions:

Figure 1: Map of the $^{87}Sr/^{86}Sr$ of groundwater for the Hanford Site after Singleton et al. (2006).

Figure 2: Map of the T-TX-TY Waste Management Areas in the 200 West Area, Hanford, WA. Shown are locations of vadose zone boreholes including the studied borehole cores C4104 and C3832. Locations of groundwater sampling wells, and the location of the multi-level well W11-25B are also shown. For brevity, the 299- prefix has been dropped from well names. Contours of ^{99}Tc groundwater concentration from Hartman et al. (2006).

Figure 3: Profiles for the C3832 (panel A) and C4104 (panel B) cores of Uranium concentration and $^{236}U/^{238}U$. Uranium concentrations are from Serne et al. (2004a,b).

Figure 4: Plots of Uranium isotopic data: (A) $^{236}U/^{238}U$ vs. $^{235}U/^{238}U$; (B) $^{236}U/^{238}U$ vs. $^{234}U/^{238}U$. Black circles are data for pore water extracts from C4104 (WMA-T), pink squares are data for pore water extracts from C3832 (WMA-TX). Errors for data are approximately the size of the symbols or smaller. Red triangles represent estimates by Jones et al. (2000) of the U isotopic compositions of suspected/known tank leaks in the WMA's T-TX-TY. The blue square and green diamond represents the U isotopic compositions of the BX102 and B110 tank leaks established by Christensen et al. 2004. In A, data for a 1999 sample of W10-24 is from Dresel et al. (2002). Inset in B at expanded scale shows the best-fit line through the top four samples and its relationship to model compositions for processed enriched U fuels from Waltrous and Wootan, (1997). Numbers along best-fit line represent percentage of processed enriched fuel in the mixture.

Figure 5: Profile through core C4104 of the pore water concentrations of Sr (μg/L or ppb), nitrate (mg/L or ppm), U (μg/L or ppb) and ^{99}Tc (nCi/L). Data from Serne et al. (2004b).

Figure 6: (A) Map of groundwater $^{87}Sr/^{86}Sr$ in the WMA T-TX-TY and vicinity. Data from Table 2 and Singleton et al. (2006) (B) Profile below water table in W11-25B (see Fig. 2 for location) of $^{87}Sr/^{86}Sr$. Same color scale as for A.

Figure 7: Plot of $\delta^{15}N$ vs. $\delta^{18}O$ for nitrate in groundwater samples from the WMA-T and for the sub-water table depth discrete samples from W11-25B. Additional data, the field for background cores, and data for contaminated cores (C4105 and C3832) from Singleton et al. 2005. The field for synthetic nitrate (representing low-level waste) is from Kendall (1998) and Amberger and Schmidt (1987). Lines connect samples from the same well taken at different times, with the more recent sample indicated by a white dot.

Figure 8: Plot of $^{236}U/^{238}U$ vs. pH for core C4104 in the WMA-T. Data for pH from Serne et al. (2004b).

Figure 9: Plot of depth below ground surface vs. $^{87}Sr/^{86}Sr$ comparing vadose zone pore waters from the contaminated cores C4104 (black circles) and C3832 (red squares) with vadose zone pore water from an uncontaminated core (blue diamonds, W22-48 Maher et al. 2003). Green stars represent bulk sediment analyses for W22-48 (Maher et al. 2003). Dashed lines connect corresponding stratigraphic depths for the cores. Pink shaded and purple shaded areas represent zones of U and ^{99}Tc contamination.

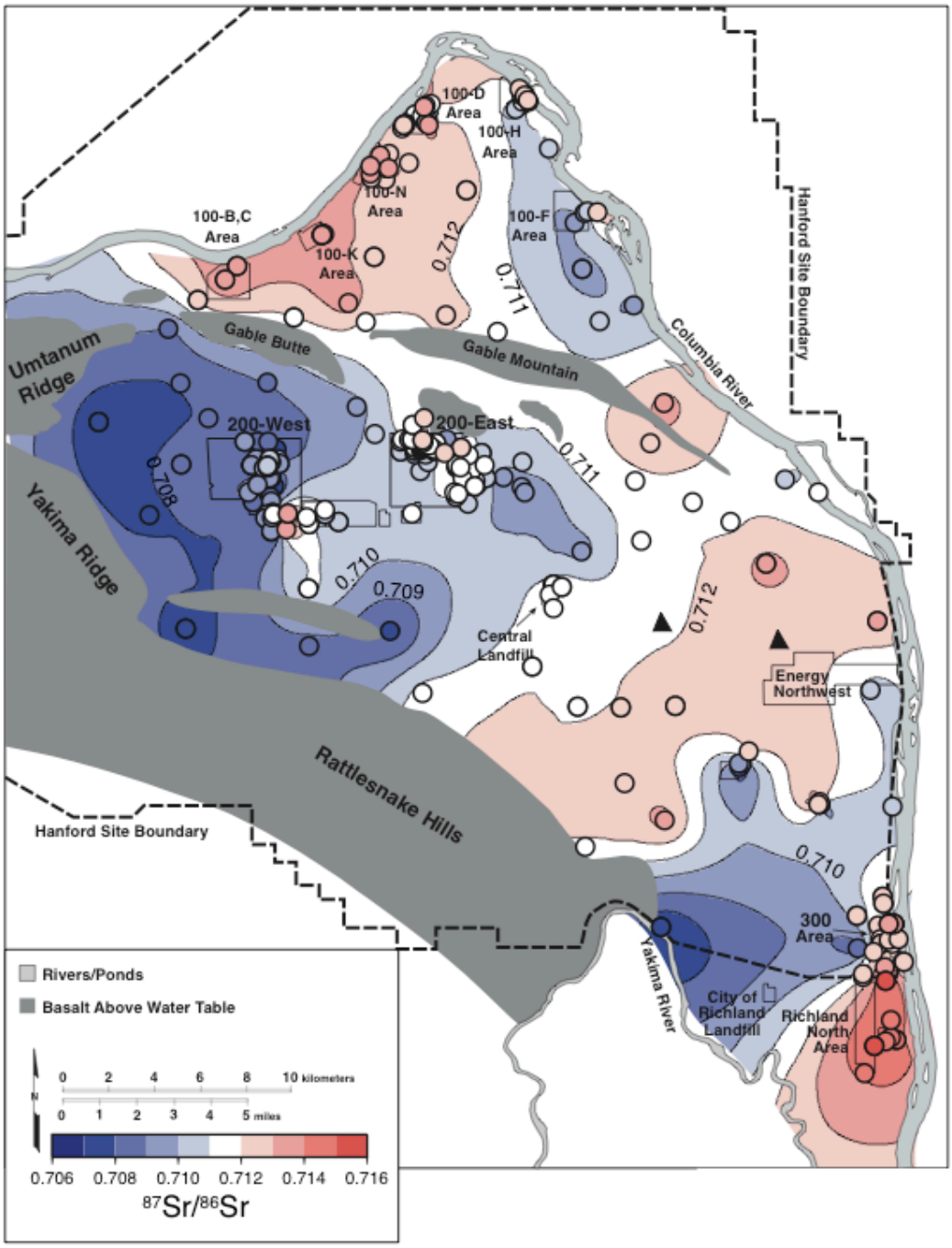
100-D Area
100-H Area
100-N Area
100-B,C Area
100-K Area
100-F Area
0.712
0.711
Hanford Site Boundary
Columbia River
Gable Butte
Gable Mountain
Umtanum Ridge
200-West
200-East
0.711
0.708
Yakima Ridge
0.710
0.709
Central Landfill
0.712
Energy Northwest
Rattlesnake Hills
Hanford Site Boundary
0.710
300 Area
Yakima River
City of Richland Landfill
Richland North Area
Rivers/Ponds
Basalt Above Water Table
0 2 4 6 8 10 kilometers
0 1 2 3 4 5 miles
0.706 0.708 0.710 0.712 0.714 0.716
87Sr/86Sr

Figure 1.

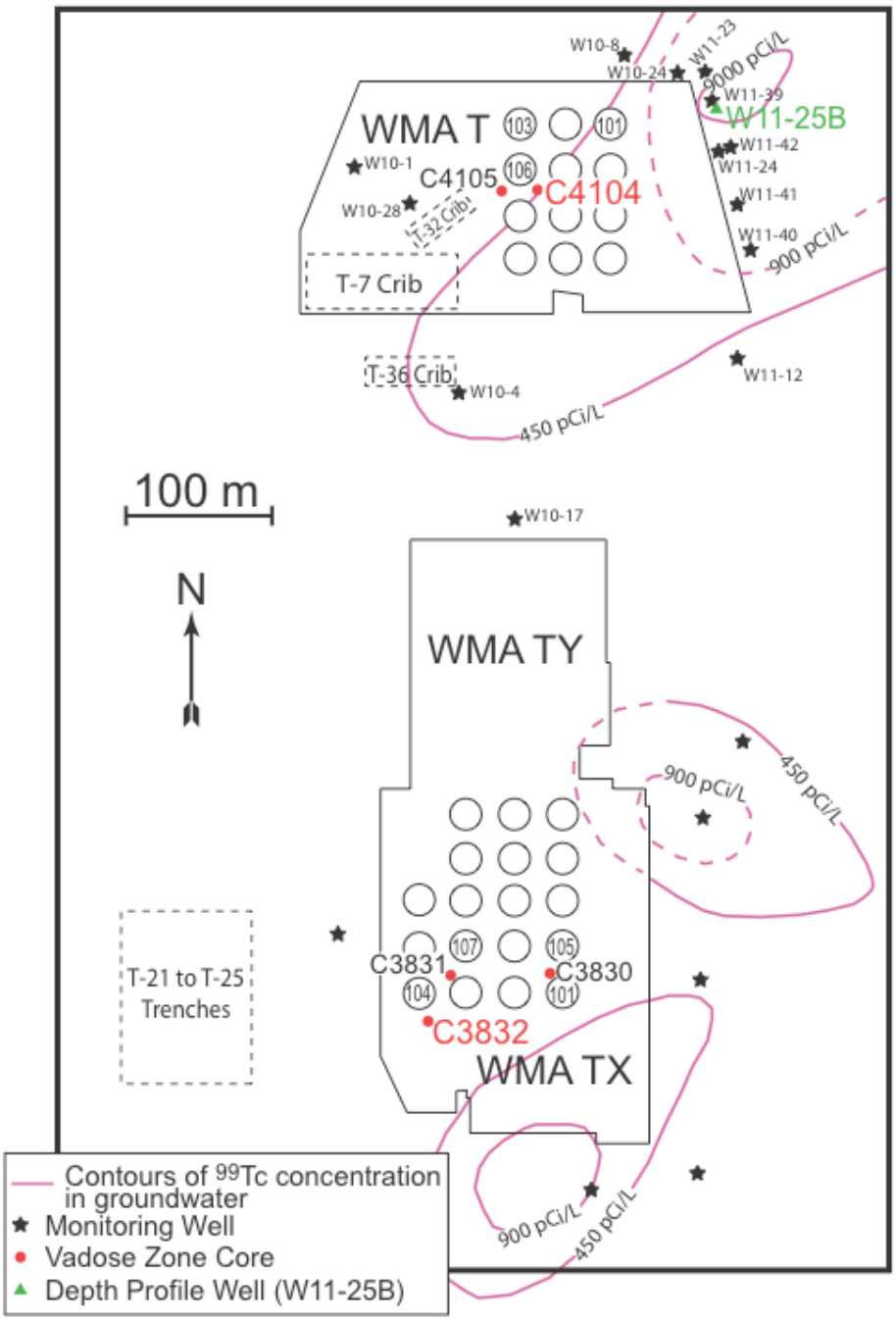
W10-8
W10-24
W11-23
9000 pCi/L
W11-39
W11-25B
WMA T
103
101
W10-1
C4105
106
C4104
W11-42
W11-24
W10-28
T-32 Crib
W11-41
W11-40
900 pCi/L
T-7 Crib
T-36 Crib
W10-4
W11-12
450 pCi/L
100 m
W10-17
N
WMA TY
900 pCi/L
450 pCi/L
T-21 to T-25
Trenches
107
105
C3831
C3830
104
101
C3832
WMA TX
900 pCi/L
450 pCi/L
Contours of 99Tc concentration in groundwater
Monitoring Well
Vadose Zone Core
Depth Profile Well (W11-25B)

Figure 2.

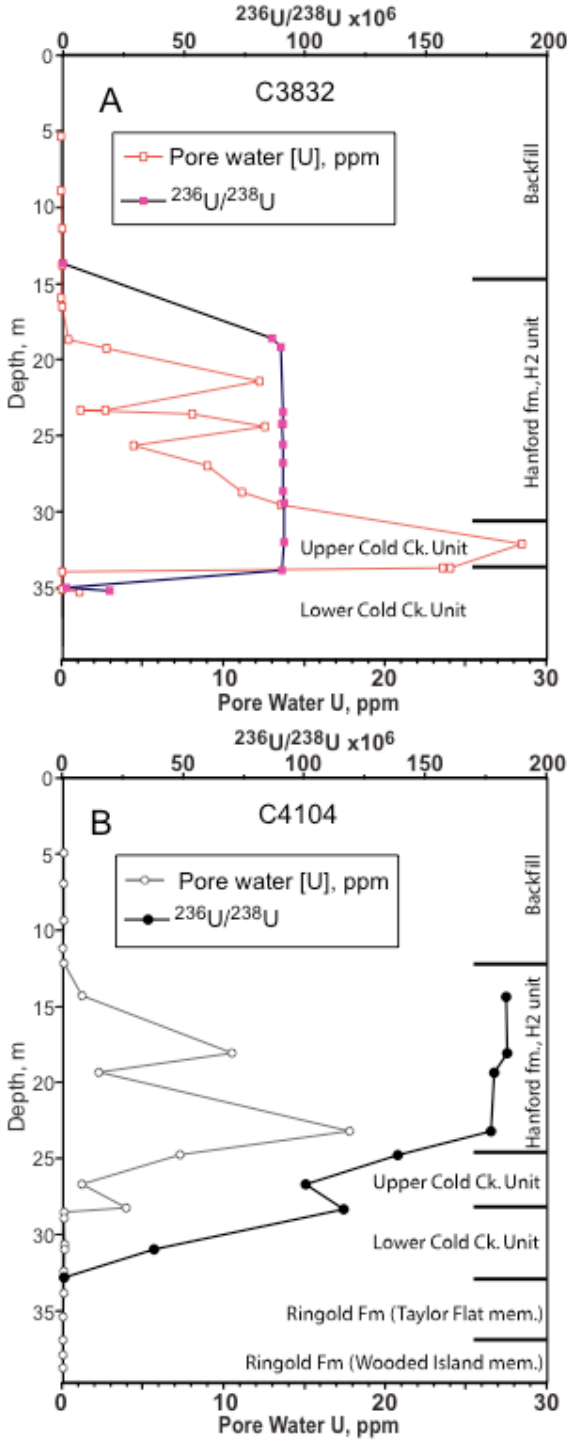
A
C3832
Pore water [U], ppm
236U/238U
236U/238U x10^6
Depth, m
Pore Water U, ppm
Backfill
Hanford fm., H2 unit
Upper Cold Ck. Unit
Lower Cold Ck. Unit
B
C4104
Pore water [U], ppm
236U/238U
236U/238U x10^6
Depth, m
Pore Water U, ppm
Backfill
Hanford fm., H2 unit
Upper Cold Ck. Unit
Lower Cold Ck. Unit
Ringold Fm (Taylor Flat mem.)
Ringold Fm (Wooded Island mem.)

Figure 3a, 3b

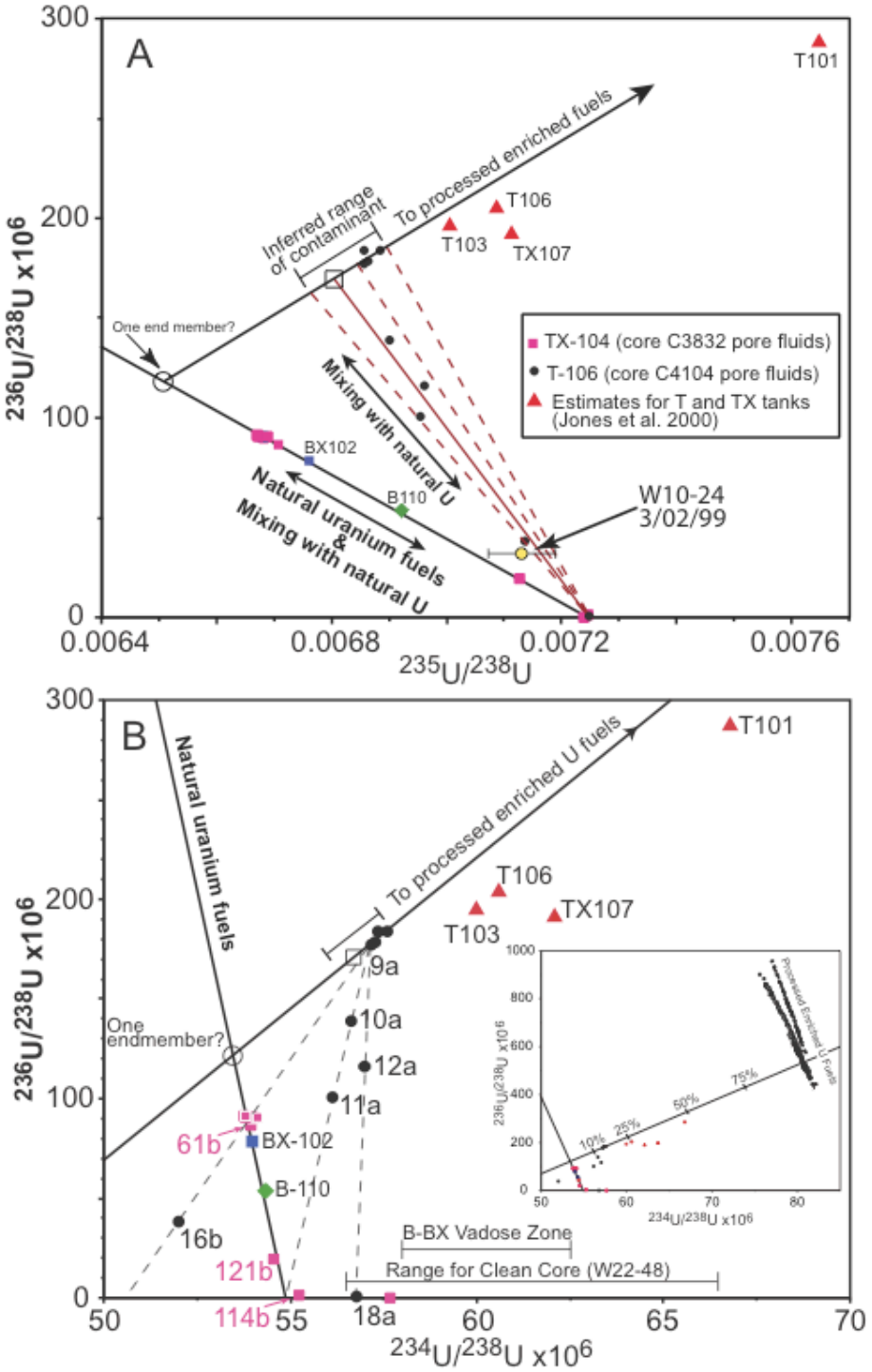
A
T101
T106
T103
TX107
To processed enriched fuels
Inferred range of contaminant
One end member?
TX-104 (core C3832 pore fluids)
T-106 (core C4104 pore fluids)
Estimates for T and TX tanks (Jones et al. 2000)
Mixing with natural U
BX102
B110
Natural uranium fuels & Mixing with natural U
W10-24 3/02/99
236U/238U x10^6
235U/238U
0.0064
0.0068
0.0072
0.0076
300
200
100
0
B
Natural uranium fuels
To processed enriched U fuels
T101
T106
TX107
T103
9a
10a
12a
11a
One endmember?
61b
BX-102
B-110
16b
121b
114b
18a
B-BX Vadose Zone
Range for Clean Core (W22-48)
234U/238U x10^6
50
55
60
65
70
Processed Enriched U Fuels
10%
25%
50%
75%

Figure 4a, 4b

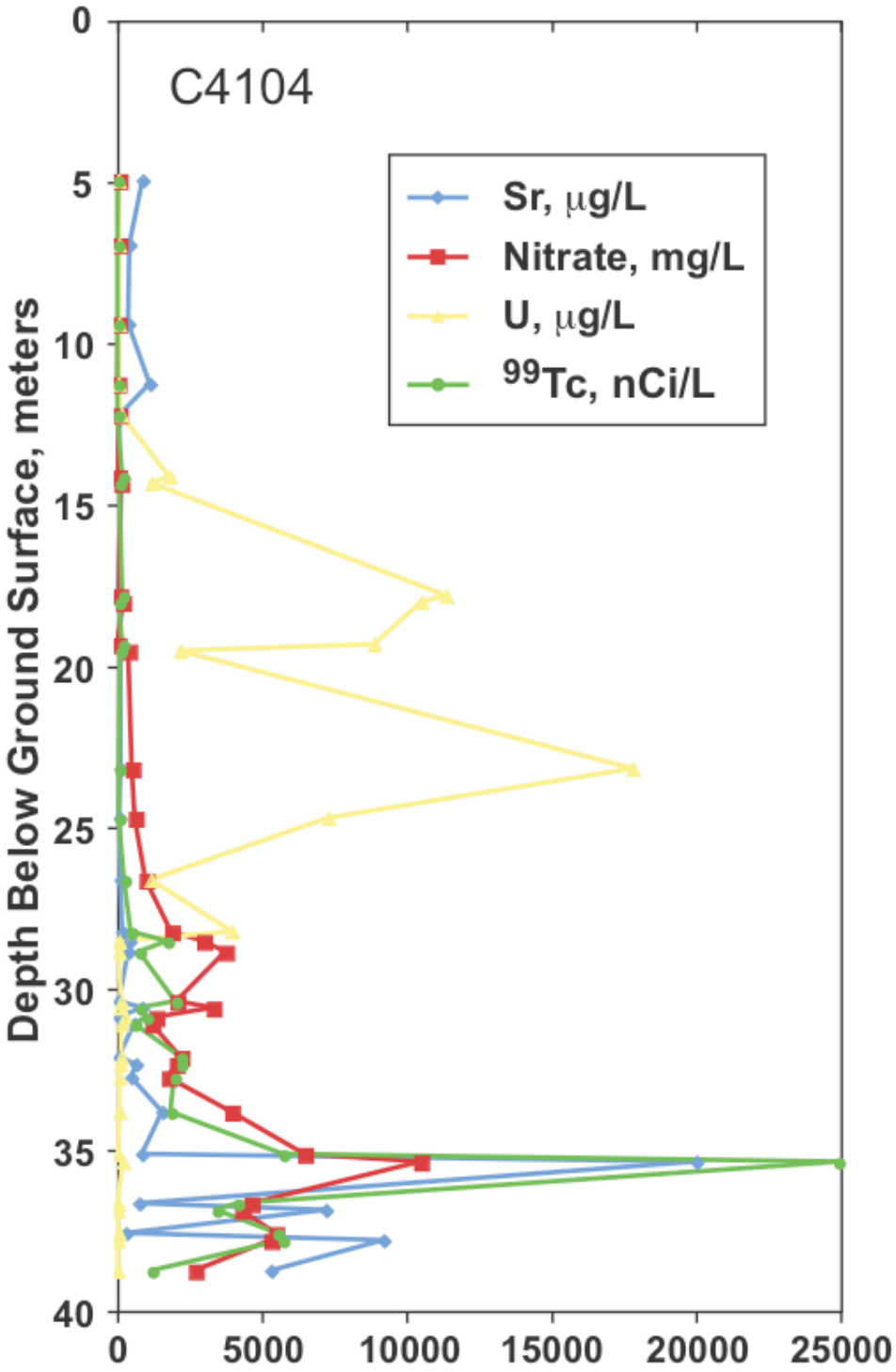
C4104
Sr, μg/L
Nitrate, mg/L
U, μg/L
99Tc, nCi/L
Depth Below Ground Surface, meters
0
5
10
15
20
25
30
35
40
0
5000
10000
15000
20000
25000

Figure 5.

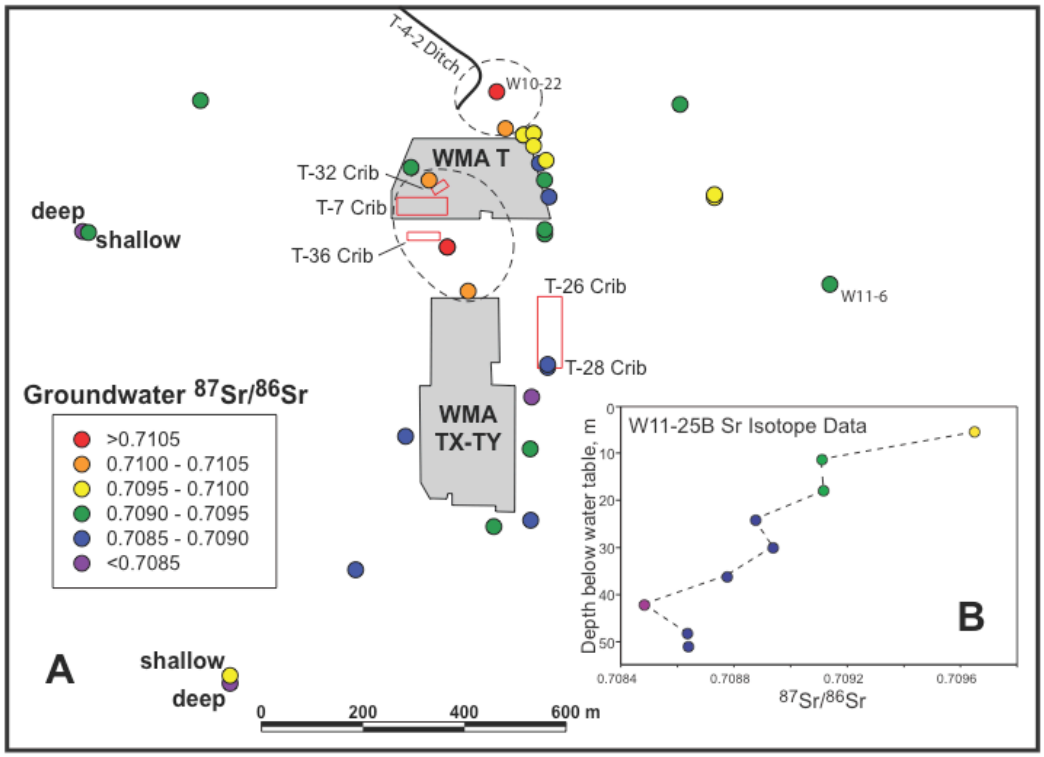
T-4-2 Ditch
W10-22
WMA T
T-32 Crib
T-7 Crib
T-36 Crib
deep
shallow
T-26 Crib
W11-6
T-28 Crib
WMA
TX-TY
Groundwater 87Sr/86Sr
>0.7105
0.7100 - 0.7105
0.7095 - 0.7100
0.7090 - 0.7095
0.7085 - 0.7090
<0.7085
A
shallow
deep
0
200
400
600 m
W11-25B Sr Isotope Data
Depth below water table, m
0
10
20
30
40
50
0.7084
0.7088
0.7092
0.7096
87Sr/86Sr
B

Figure 6a,b

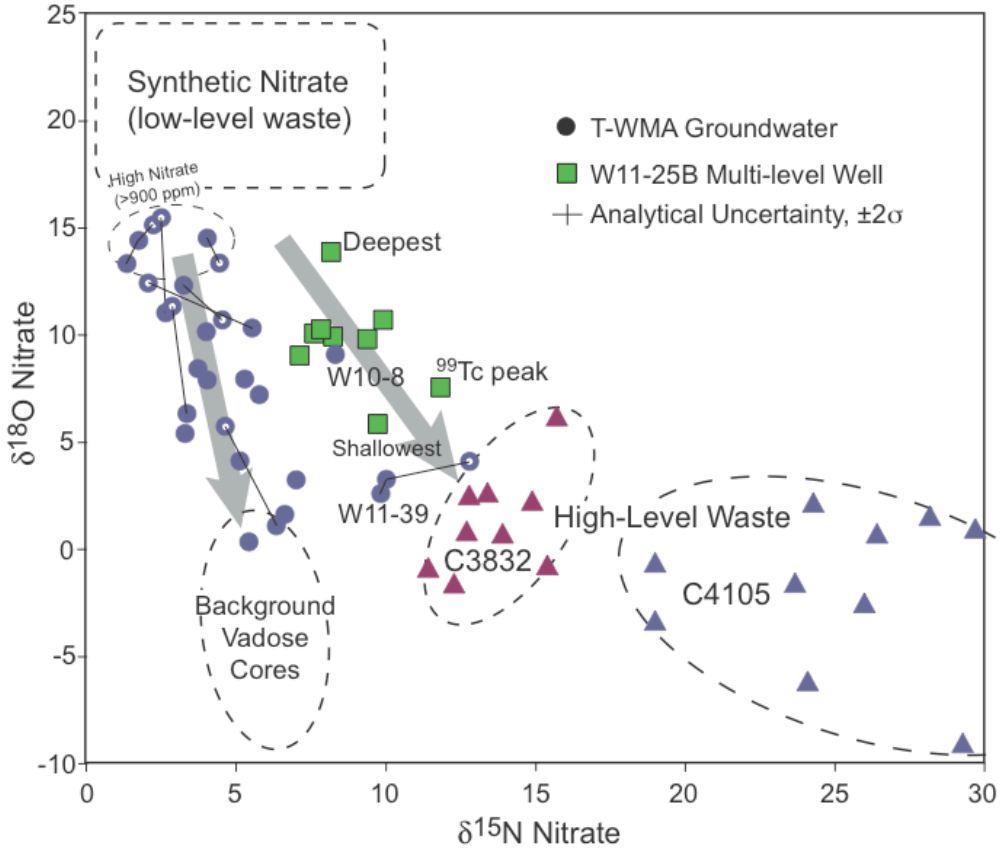
Synthetic Nitrate
(low-level waste)
High Nitrate
(>900 ppm)
T-WMA Groundwater
W11-25B Multi-level Well
Analytical Uncertainty, ±2σ
Deepest
W10-8
99Tc peak
Shallowest
W11-39
High-Level Waste
C3832
C4105
Background
Vadose
Cores
δ18O Nitrate
δ15N Nitrate
25
20
15
10
5
0
-5
-10
0
5
10
15
20
25
30

Figure 7.

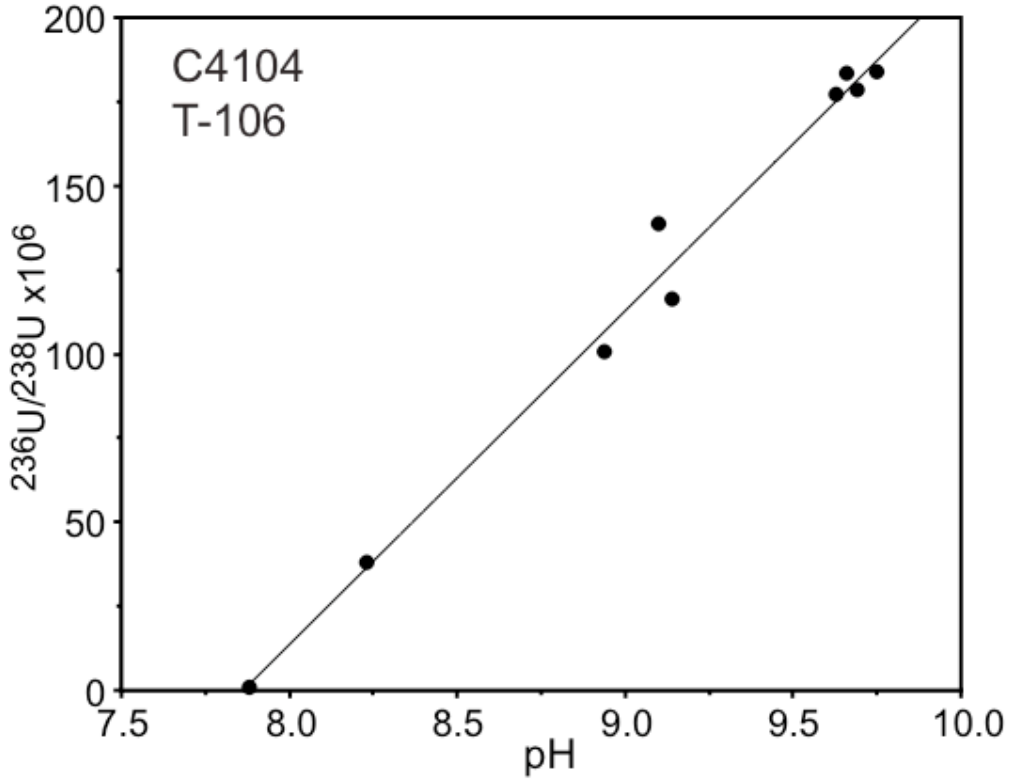

Figure 8.

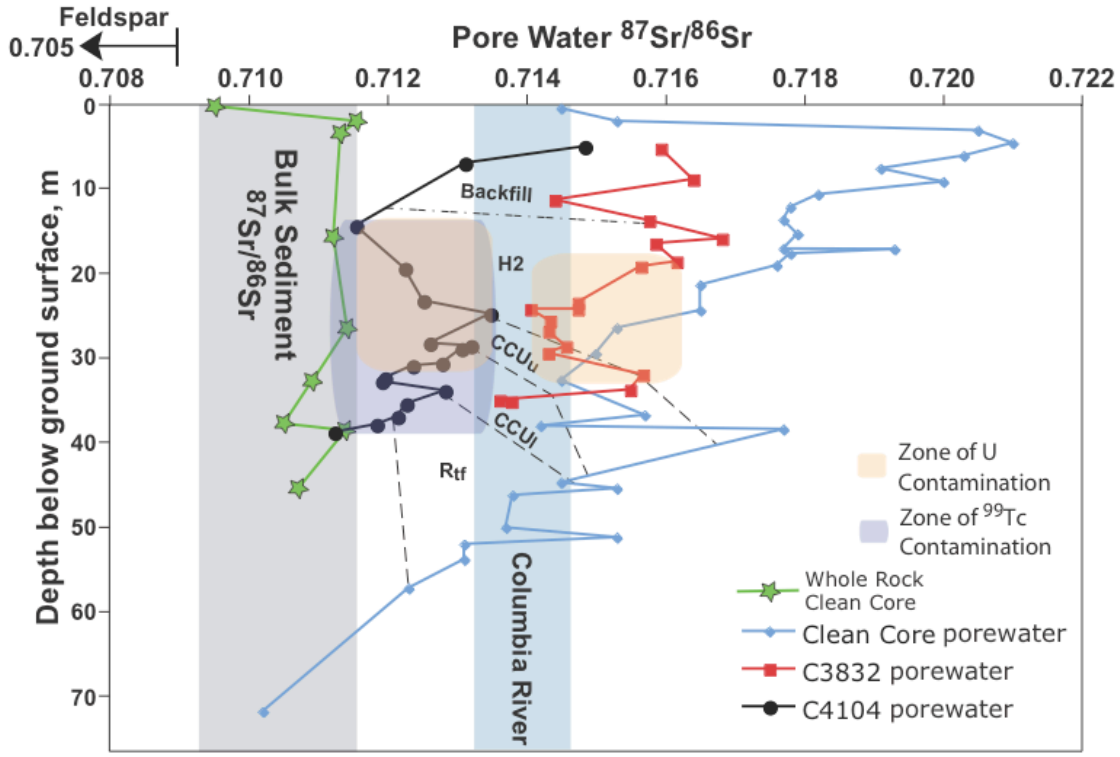
Feldspar
0.705
Pore Water 87Sr/86Sr
0.708
0.710
0.712
0.714
0.716
0.718
0.720
0.722
Depth below ground surface, m
0
10
20
30
40
50
60
70
Bulk Sediment 87Sr/86Sr
Backfill
H2
CCUu
CCUl
Rtf
Columbia River
Zone of U Contamination
Zone of 99Tc Contamination
Whole Rock Clean Core
Clean Core porewater
C3832 porewater
C4104 porewater

Figure 9.

Table 1a (C3832)

sample #	Depth BGS, m	$^{87}Sr/^{86}Sr$	±2σ	[Sr] ppm†	$^{234}U/^{238}U$ x10^6	±2σ	$^{235}U/^{238}U$	±2σ	$^{236}U/^{238}U$ x10^6	±2σ	[U]. ppm†
C3238-15B	5.15	0.715930	0.000013	0.75							
C3238-28B	8.78	0.716396	0.000010	1.18							
C3238-37B	11.22	0.714407	0.000009	0.58							0.113
C3238-44B	13.66	0.715761	0.000014	0.35	57.67	0.05	0.0072379	0.0000058	0.096	0.002	0.071
C3238-52B	15.82	0.716813	0.000011	0.34							0.019
C3238-53B	16.40	0.715854	0.000014	0.21							0.042
C3238-61B	18.54	0.716158	0.000010	0.50	53.96	0.08	0.0067069	0.0000022	86.50	0.08	0.407
C3832-62B	19.08	0.715647	0.000011	0.11	53.96	0.15	0.0066828	0.0000043	90.13	0.07	2.66
C3832-69B	23.38	0.714739	0.000009	0.20	54.11	0.06	0.0066877	0.0000018	90.66	0.13	
C3832-76B	24.18	0.714739	0.000009	0.32	54.00	0.06	0.0066814	0.0000035	90.66	0.13	2.78
C3832-79B	24.18	0.714052	0.000011	0.67	53.80	0.05	0.0066807	0.0000024	90.44	0.13	12.82
C3832-83B	25.52	0.714334	0.000011	0.63	53.82	0.08	0.0066734	0.0000015	90.66	0.13	7.38
C3238-87B	26.74	0.714317	0.000009	0.63	53.77	0.08	0.0066731	0.0000018	90.99	0.12	9.58
C3238-93B	28.57	0.714568	0.000009	0.59	53.97	0.06	0.0066882	0.0000031	90.79	0.13	5.65
C3238-96B	29.36	0.714310	0.000010	0.78	53.81	0.05	0.0066727	0.0000019	91.30	0.08	12.06
C3238-104B	31.92	0.715670	0.000010	1.42	53.77	0.10	0.0066701	0.0000027	91.37	0.16	22.53
C3238-110B	33.72	0.715487	0.000010	1.61	53.83	0.06	0.0066768	0.0000019	90.48	0.13	23.85
C3238-114B	34.91	0.713610	0.000009	2.81	55.24	0.12	0.0072463	0.0000042	1.22	0.01	0.051
C3238-121B	35.12	0.713779	0.000011	2.38	54.54	0.11	0.0071269	0.0000047	19.31	0.04	0.043

†From Serne et al. (2004a)

Table 1b (C4104)

Sample	Depth BGS, m	$^{87}Sr/^{86}Sr$	±2σ	[Sr] ppm†	$^{234}U/^{238}U$ x10^6	±2σ	$^{235}U/^{238}U$	±2σ	$^{236}U/^{238}U$ x10^6	±2σ	[U] ppm†
C4104-1a	4.93	0.714836	0.000009	0.86							0.031
C4104-2a	6.92	0.713107	0.000013	0.41							0.037
C4104-6a	14.32	0.711543	0.000010	0.15	57.59	0.08	0.0068840	0.0000025	183.59	0.18	1.18
C4104-7a	18.01			0.20	57.33	0.06	0.0068577	0.0000017	184.08	0.30	10.50
C4104-8b	19.32	0.712244	0.000027	0.11	57.28	0.09	0.0068644	0.0000025	178.35	0.33	2.24
C4104-9a	23.17	0.712514	0.000010	0.11	57.19	0.08	0.0068555	0.0000022	177.22	0.54	17.80
C4104-10a	24.70	0.713477	0.000063	0.06	56.64	0.11	0.0068999	0.0000037	138.63	0.24	7.27
C4104-11a	26.62			0.10	56.13	0.07	0.0069556	0.0000032	100.65	0.11	1.15
C4104-12a	28.23	0.712605	0.000011	0.16	57.00	0.14	0.0069607	0.0000051	116.20	0.18	3.94
C4104-13a	28.52	0.713192	0.000009	0.41							0.044
C4104-14a	28.86	0.713064	0.000009	0.37							0.048
C4104-15a	30.59	0.712779	0.000009	0.85							0.092
C4104-16b	30.89	0.712357	0.000013	0.58	52.00	0.06	0.0071368	0.0000018	38.03	0.09	0.115
C4104-17a	32.34	0.711956	0.000026	0.63							0.077
C4104-18a	32.74	0.711911	0.000021	0.47	56.77	0.09	0.0072487	0.0000028	0.94	0.01	0.053
C4104-19a	33.83	0.712821	0.000011	1.40							0.043
C4104-20a	35.36	0.712265	0.000010	20.00							0.019
C4104-21a	36.87	0.712139	0.000011	7.20							0.004
C4104-22a	37.81	0.711836	0.000010	9.20							0.003
C4104-23a	38.75	0.711232	0.000010	5.30							0.005

†From Serne et al. (2004b)

Table 2.

Well	Depth BWT, m	Sample Date	^{99}Tc, pCi/L*	$[NO3^-]$ ppm*	$\delta^{15}N_{NO3}$	$\delta^{18}O_{NO3}$	$^{87}Sr/^{86}Sr$	±2σ	[Sr] ppm
299-W10-1	~0	5/9/05	81	126	5.3	8.0			
299-W10-1	~0	2/4/05	75	132			0.708690	0.000009	0.288
299-W10-22	~0	5/9/05	129	292	2.8	11.3			
299-W10-24	~0	2/7/05	1470	400	5.5	10.3	0.709529	0.000010	0.089
299-W10-24	~0	5/9/05	1220	319	2.0	12.4			
299-W10-28	~0	2/4/05	258	1540	4.0	14.5	0.710008	0.000009	1.55
299-W10-28	~0	5/9/05	310	1660	4.4	13.4			
299-W10-4	~0	2/7/05	876	2420	2.4	15.4	0.710751	0.000011	2.39
299-W10-8	~0	6/13/05	91	192	8.3	9.2			
299-W11-12	~0	5/10/05	167	109	7.0	3.3			
299-W11-39	~0	2/11/05	12200	113	9.8	2.6	0.709681	0.000009	0.359
299-W11-39	~0	5/10/05	27400	157	12.8	4.1			
299-W11-40	~0	2/7/05	1440	207	6.3	1.1	0.709243	0.000010	0.384
299-W11-40	~0	5/12/05	2050	243	4.6	5.7			
299-W11-41	~0	2/7/05	3270	850	4.5	10.7	0.708719	0.000010	0.456
299-W11-42	~0	2/8/05	1910	1120	1.3	13.3	0.708828	0.000010	0.249
299-W11-42	~0	5/10/05	1740	832	2.2	15.2			
299-W11-7	~0	5/12/05	422	147	5.7	7.3			
W11-25B	5.5	2/8/05	77010	372	9.7	5.9	0.7096515	0.000024	0.607
W11-25B	11.3	2/8/05	151810	569	11.8	7.6	0.7091092	0.000010	0.438
W11-25B	18.0	2/16/05	54740	427	9.4	9.9	0.7091178	0.000011	0.296
W11-25B	24.1	2/17/05	49810	404	7.6	10.1	0.7088733	0.000011	0.232
W11-25B	29.9	2/23/05	42330	415	9.9	10.8	0.7089387	0.000011	0.262
W11-25B	36.0	2/24/05	37740	409	7.1	9.1	0.7087739	0.000013	0.301
W11-25B	42.1	3/4/05	25160	335	8.2	10.0	0.7084827	0.000011	0.305
W11-25B	48.2	3/7/05	30770	370	7.8	10.3	0.708635	0.000011	0.288
W11-25B	50.9	3/8/05	21250	374	8.2	13.9	0.7086373	0.000011	0.274

*From Hartman et al. (2005)

Table 3.

Well	Sample Date	Depth below water table, m	$^{234}U/^{238}U$ x10^6	±2σ	$^{235}U/^{238}U$	±2σ	$^{236}U/^{238}U$ x10^6	±2σ
W10-24	2/7/05	~0	88.15	0.11	0.0072587	0.0000040	0.348	0.008
W10-28	2/4/05	~0	74.13	0.08	0.0072468	0.0000034	0.176	0.003
W11-39	2/11/05	~0	88.72	0.11	0.0072393	0.0000044	0.046	0.003
W11-25B	2/8/05	11.3	92.28	0.09	0.0072556	0.0000035	0.184	0.006
W11-25B	2/23/05	29.9	96.49	0.08	0.0072508	0.0000034	0.118	0.003
W11-25B	2/24/05	36.0	93.51	0.09	0.0072580	0.0000035	0.418	0.005